



Superconducting transition temperatures in the electronic and magnetic phase diagrams of $\text{Sr}_2\text{VFeAsO}_{3-\delta}$, a superconductor

Yujiro Tojo¹, Taizo Shibuya^{2,8}, Tetsuro Nakamura¹, Koichiro Shoji¹, Hiroataka Fujioka¹, Masanori Matoba¹, Shintaro Yasui³, Mitsuru Itoh³, Soshi Iimura^{3,4}, Hidenori Hiramatsu^{3,4}, Hideo Hosono^{3,4}, Shigeto Hirai^{5,6,9}, Wendy Mao^{5,6}, Shinji Kitao⁷, Makoto Seto⁷ and Yoichi Kamihara^{1,10}

¹ Department of Applied Physics and Physico-Informatics, Keio University, Yokohama 223-8522, Japan

² Department of Mechanical Engineering, Keio University, Yokohama 223-8522, Japan

³ Laboratory for Materials and Structures, Tokyo Institute of Technology, 4259 Nagatsuta, Yokohama 226-8503, Japan

⁴ Materials Research Center for Element Strategy, Tokyo Institute of Technology, 4259 Nagatsuta, Midori-ku, Yokohama 226-8503, Japan

⁵ Department of Geological Sciences, Stanford University, CA 94305, United States of America

⁶ SLAC National Accelerator Laboratory, Stanford Institute for Materials and Energy Sciences, 2575 Sand Hill Road, Menlo Park, CA 94025, United States of America

⁷ Institute for Integrated Radiation and Nuclear Science, Kyoto University, Kumatori-cho, Sennan-gun, Osaka 590-0494, Japan

E-mail: kamihara_yoichi@keio.jp

Received 22 February 2018, revised 15 November 2018

Accepted for publication 11 December 2018

Published 23 January 2019

Abstract

We elucidate the magnetic phases and superconducting (SC) transition temperatures (T_c) in $\text{Sr}_2\text{VFeAsO}_{3-\delta}$ (21113V), an iron-based superconductor with a thick-blocking layer fabricated from a perovskite-related transition metal oxide. At low temperatures ($T < 37.1$ K), 21113V exhibited a SC phase in the range $0.031 \leq \delta \leq 0.145$ and an antiferromagnetic (AFM) iron sublattice in the range $0.267 \leq \delta \leq 0.664$. Mixed-valent vanadium exhibited a dominant AFM phase in $0.031 \leq \delta \leq 0.088$, and a partial ferrimagnetic (Ferri.) phase in the range $0.124 \leq \delta \leq 0.664$. The Ferri. phase was the most dominant at a δ value of 0.267, showing an AFM phase of Fe at $T < 20$ K. Increasing the spontaneous magnetic moments reduced the magnetic shielding volume fraction due to the SC phase. This result was attributed to the magnetic phase of vanadium, which dominates the superconductivity of Fe in 21113V. The T_c - δ curve showed two maxima. The smaller and larger of T_c maxima occurred at $\delta = 0.073$ and $\delta = 0.145$, respectively; the latter resides on the phase boundary between AFM and the partial Ferri. phases of vanadium. 21113V is a useful platform for verifying new mechanisms of T_c enhancement in iron-based superconductors.

⁸ Present address: IoT Devices Research Laboratories, NEC Corporation, Tsukuba, Ibaraki 305-8501, Japan.

⁹ Present address: Department of Materials Science and Engineering, Kitami Institute of Technology, Kitami, Hokkaido 090-8507, Japan.

¹⁰ Author to whom any correspondence should be addressed.

Keywords: iron-based superconductors, layered perovskite-type oxide, oxygen deficiency, antiferromagnetism, phase diagram, $\text{Sr}_2\text{VFeAsO}_{3-\delta}$

1. Introduction

1.1. Backgrounds of iron-based high- T_c superconductors, $\text{Ae}_2\text{MFePnO}_{3-\delta}$

The discovery of high-temperature iron-based superconductors in mixed anion layered compounds (MALCs) [1–5] has triggered the search for superconducting (SC) materials. Considerable attention has been devoted to the newly developed superconductors with Fe square lattices. In 2009, the $\text{Ae}_2\text{MFePnO}_3$ family of SC layered iron pnictides was reported (the so-called 21113 systems), characterized by a perovskite-type layered local structure of Ae_2MO_3 , where Ae denotes an alkaline-earth metal, M denotes Sc, Ti, Cr, V or another transition metal and Pn denotes P or As. The onset temperatures (T_c^{onset}) of the SC transitions of nominally synthesized $\text{Sr}_2\text{ScFePO}_3$ and $\text{Sr}_2\text{VFeAsO}_3$ are 17 K [6] and 37.2 K [7], respectively. However several 21113 systems have been reported that they exhibit no SC phase unless M^{3+} is substituted with Ti^{4+} [8–15]. Other promising candidates for superconductivity applications are $\text{Sr}_3\text{Sc}_2\text{Fe}_2\text{As}_2\text{O}_5$ [16, 17]; a member of the so-called 32225 systems), and a homologous series of compounds [18, 19], which present perovskite-related blocking layers thicker than the 21113 systems. These backgrounds are detailed in section 1 of supplementary information (available online at stacks.iop.org/JPhysCM/31/115801/mmedia).

Amongst the 21113 compounds, $\text{Sr}_2\text{VFeAsO}_{3-\delta}$ is an attractive SC material for practical use because its large upper critical magnetic field ($\mu_0 H_{c2}$) [7, 20] is suitable for applications involving high magnetic fields. As shown in figure 1(a), the crystal structure of $\text{Sr}_2\text{VFeAsO}_{3-\delta}$ is a tetragonal lattice with the FeAs carrier-conducting layers sandwiched between the $\text{Sr}_2\text{VO}_{3-\delta}$ perovskite-related carrier-blocking layers. $\text{Sr}_2\text{VFeAsO}_{3-\delta}$ compounds with nominal chemical compositions, undergo SC transitions at $T_c^{\text{onset}} \leq 37.2$ K [7, 20–26] under ambient pressure and at $T_c^{\text{onset}} = 46.0$ K [21] under high pressure. Munevar *et al* [26] and Hummel *et al* [27] reported a quadrupole doublet in the ^{57}Fe Mössbauer spectra (MS) of SC $\text{Sr}_2\text{VFeAsO}_{3-\delta}$ at 1.5–300 K, indicating no spontaneous magnetic moment in the Fe sublattice. In contrast, the ^{57}Fe Mössbauer spectrum of normally conducting $\text{Sr}_2\text{ScFeAsO}_3$ [26] exhibits sextet lines, indicating a finite internal magnetic field induced by the magnetic moments of the Fe sublattice, whereas that of $\text{Sr}_2\text{CrFeAsO}_3$ [28] shows substantial broadening at 4.2 K, which can be fitted to various internal magnetic fields. The ^{57}Fe MS of $\text{Sr}_2\text{MFeAsO}_3$ ($M = \text{Sc}, \text{Cr}$) suggest a magnetic phase of the Fe sublattice in $\text{Sr}_2\text{VFeAsO}_{3-\delta}$ but current reports are controversial [20, 22–24, 26, 27, 29]. Therefore, constructing the magnetic and electronic phase

diagrams of $\text{Sr}_2\text{VFeAsO}_{3-\delta}$ requires a systematic study of the chemical compositions and element-specific magnetic measurements of the family.

1.2. Overview of the present study on SC $\text{Sr}_2\text{VFeAsO}_{3-\delta}$

In this study, polycrystalline $\text{Sr}_2\text{VFeAsO}_{3-\delta}$ samples containing secondary phases were prepared with various δ . In general, verifying the oxygen contents in polycrystalline samples containing second phases is a difficult task. Moreover, the transport properties and magnetism in such polycrystalline samples cannot be ignored without reasonable assumptions. In the present study, the δ values are determined from the linear relationship between δ and the lattice volume V . The reliability of the δ estimates can be checked by the chemical shift values, defined by the peak positions of vanadium $K\alpha$ radiation in x-ray fluorescence (XRF) spectra, which indirectly quantify the oxygen contents in $\text{Sr}_2\text{VFeAsO}_{3-\delta}$. The obtained samples were characterised by x-ray diffraction (XRD), XRF, ^{57}Fe Mössbauer spectroscopy [30] and thermal gas desorption. The SC and magnetic phase transition temperatures of the samples were clarified in resistivity (ρ) and magnetic moment measurements at various temperatures (T). Normally conducting samples with $0.267 \leq \delta \leq 0.664$ exhibited an antiferromagnetic (AFM) phase of Fe. The topological difference between the magnetic Fe phase and the SC phase is similar to those of other high- T_c superconductors, including $\text{ReFeAsO}_{1-x}(\text{F}, \text{H})_x$ (Re : rare earth) [31, 32] and $\text{YBa}_2\text{Cu}_3\text{O}_{7-\delta}$ [33–35]. Meanwhile, samples in the $0.031 \leq \delta \leq 0.267$ and $0.124 \leq \delta \leq 0.664$ ranges exhibit a dominant and/or partial AFM phase of V and a partial and/or dominant ferrimagnetic (Ferri.) phase of the V, respectively. Our interpretations are supported by density functional theory (DFT) calculations in the magnetic phase of $\text{Sr}_2\text{VFeAsO}_{3-\delta}$ [23].

In the earlier reports [7, 20–27, 29], an electronic and magnetic phase of $\text{Sr}_2\text{VFeAsO}_{3-\delta}$ had been controversial due to an absence of a simplified assumption that determine chemical compositions of the polycrystalline samples based on analytical chemical approach; e.g. volume Vegard’s rules (VVR) [36]. Using analogy of the VVR, present study newly introduces a verifiable relation between lattice volume V and intrinsic δ and successfully demonstrates element-specific electronic and magnetic phase diagram for $\text{Sr}_2\text{VFeAsO}_{3-\delta}$. (see figure 10)

The T_c versus δ plot displays two maxima. The lower maximum coexists with the AFM phase of the V sublattice, and the higher maximum appears near the boundary between the AFM and the Ferri. phases of the V sublattice. In the T_c

versus δ plot, AFM phase of the Fe sublattice exists separately from the SC phase. Electronic and magnetic phase of the Fe sublattice is in accord to Goodenough’s empirical consideration ‘ T - b diagram’ [37]. The present T_c versus δ plot, which is dominated by Fe 3d electrons and V 3d electrons, has updated the ‘ T - b diagram’ on more complex electronic phases of d -electrons empirically. These results clarify a topology between the superconductivity and the magnetism in MALCs with perovskite-related magnetic oxide layers.

2. Experimental

2.1. Sample preparation and characterization

Polycrystalline samples were prepared by the two-step solid-state reaction process in a sealed silica tube. The starting materials were dehydrated SrO, FeAs, V₂O₅, and V. The dehydrated SrO was prepared by heating commercial Sr(OH)₂·8H₂O powder (Sigma Aldrich Japan Co. Ltd; 99.995 wt.%) at 900°C for 10h in air. The FeAs powder, was obtained by mixing Fe (Ko-jundo Chemical Laboratory; ≥99.99 wt.%) and As (Ko-jundo Chemical Laboratory; 99.9999 wt.%) in a stoichiometric ratio of 1:1 and by heating the mixture at 600 °C for 10h in an evacuated silica tube. The FeAs were then mixed with the dehydrated SrO, V₂O₅ (Sigma Aldrich Japan Co. Ltd; 99.99 wt.%), and V (Sigma Aldrich Japan Co. Ltd; 99.9 wt.%) in the formula Sr₂VFeAsO_{3- δ} . The resulting powder was pressed into a pellet. The last two procedures were carried out in an Ar-filled glove box (MIWA Mfg; O₂, H₂O ≤ 1 ppm). The pellet was loaded into an alumina boat, sealed in an evacuated silica tube and heated to 1050 °C–1300 °C at 30 °C h⁻¹. After maintainance at the target temperature for 20h, the pellet was slowly cooled to room temperature (RT). The sample surfaces were polished using with SiC-coated abrasive paper sheets (Sankyo Rikagaku Co. Ltd; grit nos. 400 and 1000). The phase purity and lattice constants of the resulting powders were examined by powder XRD (Rigaku; RINT2500Ultra18) using Cu K α radiation from a rotating anode. The samples were scanned at RT, and the lattice constants were obtained by the least-squares fitting method. Rietveld refinement was performed by the RIETAN-FP-Venus program [38]. Our analysis procedures are summarized in section 2 of supplementary information. (see figures S1–S3).

The low temperature XRD (LTXRD) measurements were performed with synchrotron radiation at beamline 16-BMD of the advanced photon source (APS) in the Argonne National Laboratory (ANL). The measurements were carried out at 5 ≤ T ≤ 30 K and at 290 K using a diamond anvil cell in a cryostat. The lattice constants as functions of T (5–30 K) were obtained from the LTXRD patterns.

The oxygen contents and valence states of the vanadium ions in representative Sr₂VFeAsO_{3- δ} samples were examined by XRF using wavelength-dispersive x-ray spectrometry (WDX; Rigaku ZSX100e) and thermal gas desorption spectrometry. Our analysis procedures are summarised in section 2 of supplementary information (see figure S4).

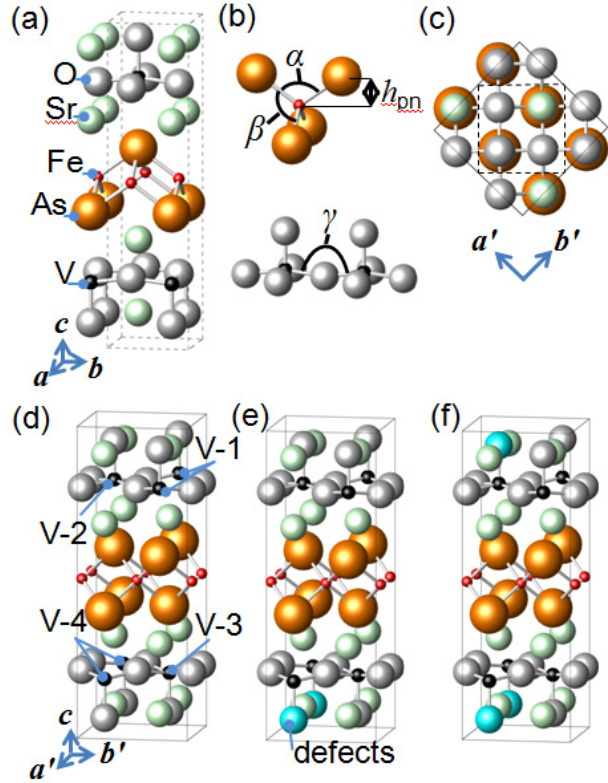


Figure 1. Crystallographic structure (a), and local structures (b) as well as supercell structures (c)–(f) of Sr₂VFeAsO_{3- δ} . (a) The dashed box represents a unit cell in the tetragonal phase. (b) Schematic of molecular FeAs₄ in the carrier-conducting FeAs layer (upper) and a VO₄ molecule in the perovskite-related Sr₂VO_{3- δ} layer (lower). Two As–Fe–As bond angles (α , β) and the distance of As from the plane formed by the Fe atoms (h_{pn}) in the FeAs layer and the V–O–V bond angle (γ) in the Sr₂VO_{3- δ} layer are illustrated. Atomic coordinations are summarized in supplementary information (see table S2). (c) Top view of the crystal structure from the c -axis direction. The dashed and solid squares represent a unit cell in the tetragonal phase and the unit cell extended to a supercell, respectively. The a -axis of the supercell is rotated by 45° from the tetragonal phase. The lattice constants a of the supercells are expanded by $\sqrt{2}$. (d)–(f) Supercell structures of Sr₂VFeAsO_{3- δ} ($\delta = 0, 0.25$ and 0.50 , respectively). In our DFT calculation, the vanadium sites were named V1, V2, V3 and V4, as shown in (d). The blue–green sites are the sites of oxygen defects in the $\delta = 0.25$ (e) and $\delta = 0.50$ (f) samples.

2.2. Macroscopic and microscopic physical property measurements

The DC electrical resistivity (ρ) was measured by a four-probe technique with Au electrodes. The ρ values of several SC samples were measured under different magnetic fluxes ($\mu_0 H = 0$ –9 T) at 2 ≤ T ≤ 300 K using a Quantum Design physical property measurement system (PPMS). The specific heats were measured at 2 ≤ T ≤ 300 K, applying a relaxation method on the PPMS. Magnetization measurements were performed on a SC quantum-interference device magnetometer (Quantum Design magnetic property measurement system) at 1.8 ≤ T ≤ 400 K, varying the magnetic flux density from –5.5

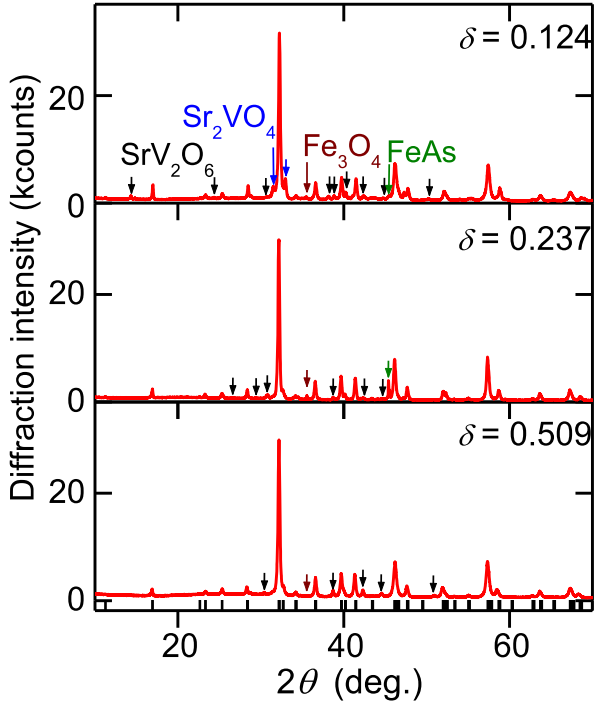


Figure 2. Powder XRD patterns of representative $\text{Sr}_2\text{VFeAsO}_{3-\delta}$ samples ($\delta = 0.124, 0.237$ and 0.509) at RT. The vertical bars at the bottom represent the calculated Bragg diffraction angles in the $\delta = 0.509$ sample. The black, blue, green and wine-red arrows represent the Bragg diffraction angles of the impurity phases SrV_2O_6 , Sr_2VO_4 , FeAs , and Fe_3O_4 , respectively.

to 5.5 T. The analysis is detailed in section 3 of supplementary information (see figure S5). The ^{57}Fe MS, measured for $\delta = 0.124, 0.232, 0.237, 0.267, 0.509$, and 0.631 samples, were obtained from 2.5 to 300 K by conventional equipment with a ^{57}Co source [30]. The isomer shift (IS) values of each sample were determined relative to that of $\alpha\text{-Fe}$. Details are given in section 4 of supplementary information (figures S6 and S7).

2.3. *Ab initio* calculations for stability of the magnetic phases

The magnetic properties of $\text{Sr}_2\text{VFeAsO}_{3-\delta}$ were evaluated in conjunction with DFT calculations under the generalized gradient approximation (the Perdew, Burke and Ernzerhof approximation [39]), using Vienna *ab initio* simulation package (VASP) code [40, 41]. To describe the checkerboard-type antiferromagnetism in the vanadium layer reported by Nakamura *et al* [42], the unit cell was extended to a 32 atom $\sqrt{2} \times \sqrt{2} \times 1$ supercell (see figures 1(c)–(f)). The core valence interaction was treated within the projector-augmented wave scheme [43]. The plane-wave cut-off energy was 500 eV, and the Brillouin zone was sampled by a $3 \times 3 \times 1$ Monkhorst-Pack grid with $\sigma = 0.05$ eV. To account for the correlated 3d orbitals of vanadium, the calculations were performed at the DFT+ U [44] level. Following Nakamura *et al* [42],

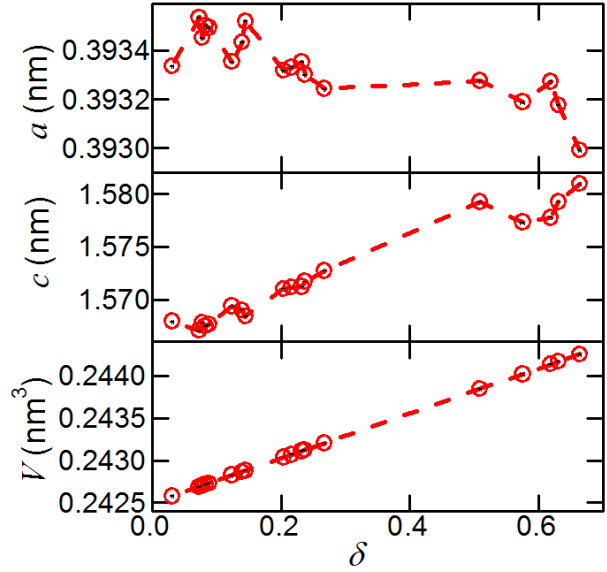


Figure 3. Lattice constants (a, c) of the $\text{Sr}_2\text{VFeAsO}_{3-\delta}$ samples at RT as functions of oxygen deficiency (δ), assuming a linear relationship between V and δ . The small black lines in the red plots are the statistical errors of our analysis. It is noted that the other errors such as temperature fluctuation (<1 K) should be considered. The δ values are determined from the lattice constants of representative samples. The XRD patterns of each sample are provided in figure S2 of supplementary information.

we set $U = 5.5$ eV and $J = 0.93$ eV. The experimental lattice constants were assumed in the calculations.

The oxygen-deficient structures ($\delta = 0.25$ and 0.50) were modelled by removing one or two 1-coordinated oxygen atoms from the supercell, as suggested by Suetin *et al* [45]. The internal coordinates were relaxed until the Hellmann-Feynman forces fell below 0.02 eV \AA^{-1} . The formation enthalpies in different magnetic configurations were evaluated by varying the initial magnetic moments on V and Fe.

3. Results

3.1. Crystallographic characterization

Figure 2 shows the powder XRD patterns of $\text{Sr}_2\text{VFeAsO}_{3-\delta}$ ($\delta = 0.124, 0.237$ and 0.509). Almost diffraction peaks are assigned to Bragg diffraction angles associated with the tetragonal $\text{Sr}_2\text{VFeAsO}_{3-\delta}$ phase, although several weak peaks could be attributed to secondary phases. The Rietveld refinement of the $\delta = 0.509$ sample revealed atomic coordination and an impurity phase content of ~ 7 vol.%. (see figure S3) The polycrystalline samples are dominated by the tetragonal $\text{Sr}_2\text{VFeAsO}_{3-\delta}$ phase. Meanwhile, the off-stoichiometry of oxygen and the appearance of secondary phases altered the chemical composition of the primary phase from the nominal. Figure 3 shows the lattice constants (a, c) and V as functions of δ at RT. As δ increased, a decreased while c increased. The a - δ curve exhibit a distinct hump (dip) at $\delta \sim 0.07$, (~ 0.12),

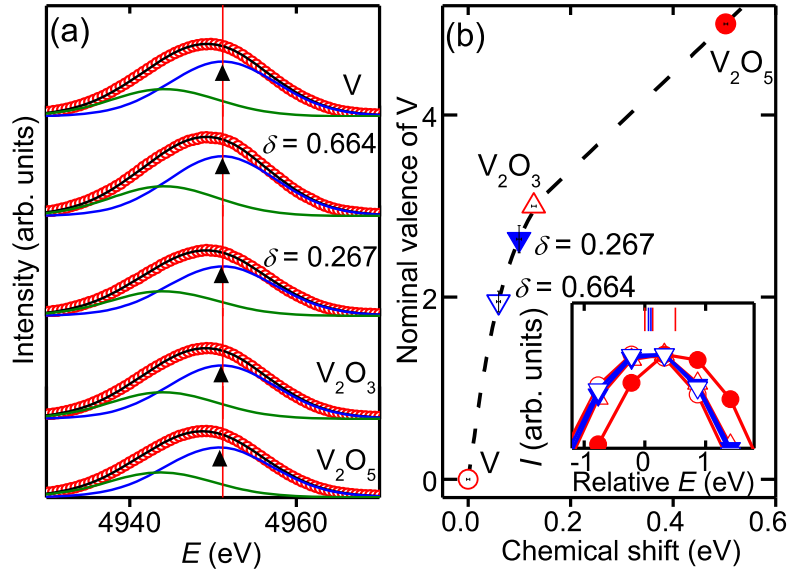


Figure 4. (a) XRF V-K α energy (E) spectra of pure vanadium metal (V), Sr₂VFeAsO_{3- δ} ($\delta = 0.267$ and 0.664), V₂O₃ and V₂O₅. Red circles are the observed data points. The black, blue and green lines denote the fitted V-K α , V-K α_1 , and V-K α_2 spectra, respectively. The vertical red line denotes E of the V-K α_1 edge of pure V (4951.170(3) eV, used as a standard). (b) Nominal valences of Sr₂VFeAsO_{3- δ} ($\delta = 0.267$ and 0.664), V₂O₃ and V₂O₅ versus the chemical shift of V-K α_1 . The dashed line is a guide for the eyes. Inset shows an expanded view of the XRF versus E (relative to that of pure V).

~ 0.14 , ~ 0.23 , (0.51), ~ 0.62 . Single-phase stoichiometric polycrystalline Sr₂VFeAsO₃ was not obtained.

3.2. Valence states of the vanadium

Figure 4(a) shows the V-K $\alpha_{1,2}$ XRF spectra of the $\delta = 0.267$ and $\delta = 0.664$ samples, pure V and vanadium oxides (V₂O₃ and V₂O₅). Each spectrum was fitted by the least-squares method. The V-K α_1 energy of Sr₂VFeAsO_{3- δ} , V₂O₃ and V₂O₅ was slightly lower than that of the pure V (4951.170(3) eV, indicated by the vertical line in figure 4(a)). The energy shifts of Sr₂VFeAsO_{3- δ} , V₂O₃ and V₂O₅ from pure V were considered to reflect the chemical shifts of the V ions in the compounds. Given the nominal valences of pure V, V₂O₃ and V₂O₅ (0, 3 and 5 respectively), the valences of $\delta = 0.267$ and $\delta = 0.664$ samples were determined as 2.6(1) and 2.0(1), respectively (figure 4(b)).

3.3. Electrical transport properties

Figure 5(a) shows the temperature (T) dependences of the electrical resistivities (ρ) of the Sr₂VFeAsO_{3- δ} samples (where $2 \leq T \leq 300$ K). The $0.204 \leq \delta \leq 0.664$ samples showed normal conductivity at $T \geq 2$ K, whereas the ρ of the $0.204 \leq \delta \leq 0.237$ samples sharply decreased at T below ~ 9 – 19 K (figure 5(a)) confirming a SC trace (figure 5(b)). That is, the $\delta = 0.204$ – 0.237 samples were chemically inhomogeneous and electronically phase-segregated, containing both major normally conducting grains and minor SC grains. The $\partial\rho/\partial T$ values of the normally conducting $0.204 \leq \delta \leq 0.237$ samples were positive at $20 \leq T \leq 300$ K, but those of the $0.509 \leq \delta \leq 0.664$ samples exhibited semiconductor-like

negative values at $T > \sim 10$ K. The ρ - T curves of the $0.267 \leq \delta \leq 0.664$ samples showed anomalous maxima (T_{\max}) at $T \sim 10$ K. As the ρ of the $0.267 \leq \delta \leq 0.664$ samples maintained a constant order of magnitude at $T < T_{\max}$, the sudden decrease at T_{\max} suggests a local crystallographic phase transition.

The ρ - T curves of the $0.031 \leq \delta \leq 0.145$ samples exhibit SC transitions at $30 \leq T_c^{\text{onset}} \leq 37$ K (figure 5(a)). In these samples, the bulk T_c can be considered as the T_c^{mid} (see table S3 in the supplementary information). The ρ - T curves of the $0.031 \leq \delta \leq 0.267$ samples exhibit an anomalous kink at ~ 200 K (denoted T_{anom} in figure 5). The T_{anom} was less well clarified in the $0.204 \leq \delta \leq 0.267$ samples with the SC trace than those of the SC $0.031 \leq \delta \leq 0.145$ samples and was absent in the normal conducting $0.509 \leq \delta \leq 0.664$ samples with no SC trace. Clearly, the T_{anom} is associated with the appearance of SC phases.

3.4. Macroscopic magnetic properties

Figure 6(a) shows the temperature dependence of the spontaneous magnetization (M_S) in the $\delta = 0.124, 0.204, 0.232, 0.237, 0.267, 0.509, 0.631$ and 0.664 samples (where $1.8 \leq T \leq 400$ K). These curves reveal the magnetic phase transition temperatures T_{ferri} of the samples, at which M_S equals to $0.01 \mu_B$ per formula unit (f.u.). The M_S values of the $0.124 \leq \delta \leq 0.664$ samples reached 0.011 – $0.53 \mu_B$ (f.u.)⁻¹ at 1.8 K. The M_S values of the $\delta = 0.124$ and 0.664 samples at 1.8 K were extrapolated by an empirical equation [46]. In the normally conducting samples, the M_S and T_{ferri} were maximized at $\delta = 0.267$ (figure 6(b)). At this composition, the M_S was sufficiently large to verify intrinsic magnetism.

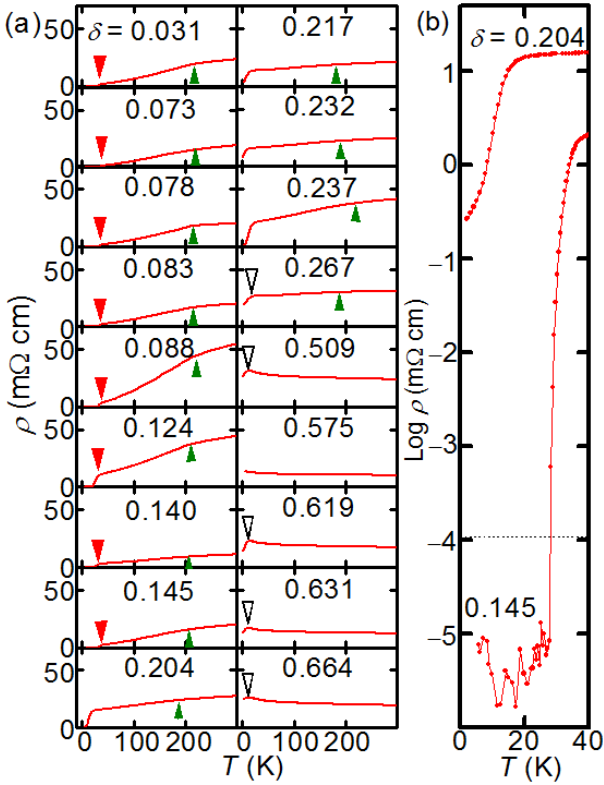


Figure 5. (a) Electrical resistivities (ρ) of the $\text{Sr}_2\text{VFeAsO}_{3-\delta}$ ($0.031 \leq \delta \leq 0.664$) samples as functions of temperature (T). Here, T is in the range 2–300 K. The δ value is indicated in each plot. The closed downward and open triangles indicate the onset temperatures of the bulk SC transition ($T_{\text{onset}}^{\text{c}}$) and the maximum temperatures of normal conductivity at 10–15 K (T_{max}) samples, respectively. The green upward triangles at ~ 200 K indicate the temperatures of the anomalous kink (T_{anom}). (b) ρ - T curves of the $\delta = 0.145$ and 0.204 samples. The dashed line denotes the detection limit of our measurement.

When the intrinsic M_S is $0.01 \mu_B$ (f.u.)⁻¹ or lower, it cannot be distinguished from extrinsic magnetic moments owing to the unknown ferromagnetic second phases. Several T_{ferri} maxima appear in the $T_{\text{ferri}} - \delta$ curve.

As shown in figure 6(c), the magnetic shielding volume fractions (SVFs) in the $\delta = 0.088, 0.124$ and 0.145 samples exceeded 10 vol.% at 1.8 K, whereas those of normal conducting samples ($0.204 \leq \delta \leq 0.237$) were below 10 vol.%. No diamagnetic susceptibility was observed in the $0.267 \leq \delta \leq 0.664$ samples. Thus, $\text{Sr}_2\text{VFeAsO}_{3-\delta}$ exhibits bulk superconductivity in the $0.031 \leq \delta \leq 0.145$ range and normal conductivity in the $0.204 \leq \delta \leq 0.664$ range.

3.5. ⁵⁷Fe MS

Figure 7 shows the temperature dependence of the ⁵⁷Fe MS of representative samples ($\delta = 0.232, 0.267,$ and 0.509). The ⁵⁷Fe MS of the other samples are presented in the supplementary information (figure S8). The ⁵⁷Fe MS of each sample exhibit quadrupole doublet absorption lines at 300 K, indicating a paramagnetic (PM) phase of the Fe sublattice. The

asymmetric doublet absorption lines derive from the anisotropic of crystal orientation [47] in $\text{Sr}_2\text{VFeAsO}_{3-\delta}$. The ⁵⁷Fe MS of the $\delta = 0.232$ sample were fitted to a doublet pattern at $2.5 \leq T \leq 300$ K with no internal magnetic field (B_{int}), indicating a PM Fe phase in this sample. In the $\delta = 0.124, 0.232$ and 0.237 samples, the PM Fe phase appeared at $T \geq 4.2$ K (see figure S6). The ⁵⁷Fe MS of the $\delta = 0.267$ and 0.509 samples were fitted to a doublet pattern from 30 to 300 K. The absorption lines broadened at $T \sim 10$ K, indicating the presence of spontaneous magnetic moments in the Fe sublattice. The broad absorption lines clearly differed from the sextet split spectrum of antiferromagnetically ordered Fe sublattices, which typify the mother compounds of iron-based superconductors, e.g. LaFeAsO [30] and BaFe_2As_2 [48]. Figure 8(a) shows the temperature dependences of the IS, quadrupole splitting (QS) and full-width at half-maximums (FWHMs) in the $\delta = 0.124, 0.232, 0.237, 0.267, 0.509$ and 0.631 samples. The FWHMs of the $\delta = 0.267, 0.509$ and 0.631 samples substantially increased at $T < 20$ K, indicating a finite distribution of B_{int} in these samples and the presence of magnetic and nonmagnetic Fe in the same chemical composition. Given the wide distribution of B_{int} , the broad absorption lines can be fitted sufficiently well to quantify the mean B_{int} . In the present study, the B_{int} distribution was obtained by Hesse and Rübertsch’s method [49]. As shown in figure 8(a), the IS value at RT was smaller in the SC $\delta = 0.124$ sample than in the normal conducting samples ($\delta = 0.232, 0.237, 0.267, 0.509$ and 0.631). This indicates higher s-electron densities around the nucleus of the $\delta = 0.124$ sample than around nuclei of the other samples. From the IS- T curves in the Debye approximation of the lattice vibrations, the Debye temperatures of the $\delta = 0.232$ and $\delta = 0.509$ samples were obtained as 454(29) K and 362(12) K respectively. The δ correlates with elastic properties of $\text{Sr}_2\text{VFeAsO}_{3-\delta}$. The IS- T curve of the $\delta = 0.509$ sample anomalously decreased with decreasing temperature at $T < 20$ K (figure 8(a), upper inset). In general, the IS of a sample with no phase transition increases and saturates at low temperatures, like the theoretical curves in figure 8(a) (upper inset). The anomalously decreasing IS indicates a transition in the $\delta = 0.509$ sample at $T < 20$ K. Indeed, several samples exhibited a kink in their QS- T curves and a sudden increase of their FWHM- T curves, indicating the presence of anisotropic electric field gradients and AFM phases of the Fe sublattice. Figure 8(b) shows the temperature (T) dependence of the square root of the mean squared-amplitude of the internal magnetic field ($\sqrt{\langle B_{\text{int}}^2 \rangle}$) induced by the AFM phase of Fe in the $\delta = 0.267, 0.509$ and 0.631 samples. The relationship between $\sqrt{\langle B_{\text{int}}^2 \rangle}$ and T follows an empirical formula [46]. The Néel temperatures (T_N) of the Fe were found to be $T_N = 16.2(4)$ K, $19.2(4)$ K and $23.3(4)$ K in the $\delta = 0.267, 0.509$ and 0.631 samples. Increasing the δ enhanced the T_N of Fe in $\text{Sr}_2\text{VFeAsO}_{3-\delta}$. The $\sqrt{\langle B_{\text{int}}^2 \rangle}$ values were 4.9(3) T, 7.9(3) T and 8.5(3) T at 0 K. Applying the conversion factor $\text{CF} = 15 \text{ T}\mu_B^{-1}$ [50], the average magnetic moments at 0 K were determined of 0.33(2), 0.53(2) and 0.57(2) $\mu_B \text{ Fe}^{-1}$ in $\delta = 0.267, 0.509$ and 0.631 samples. Statistical errors are

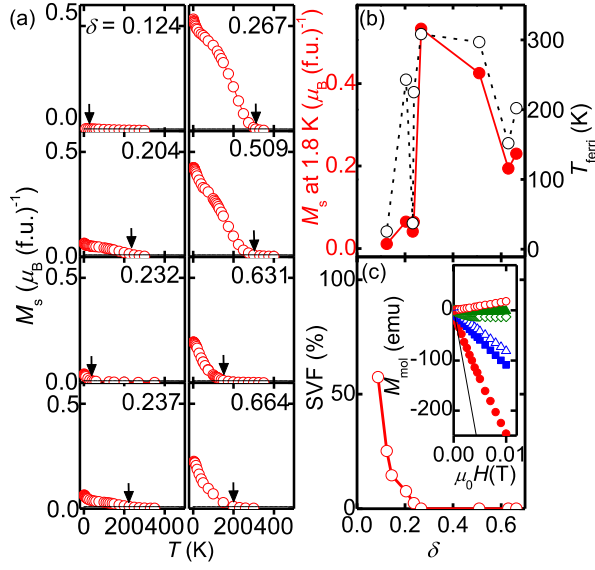


Figure 6. Magnetic properties of $\text{Sr}_2\text{VFeAsO}_{3-\delta}$. Spontaneous magnetization (M_S) are defined as linearly extrapolated values at magnetic flux density ($\mu_0 H$) = 0 tesla from magnetization in a range of $\mu_0 H = 3\text{--}5.5$ tesla. (a) M_S versus temperature (T) for the $\delta = 0.124, 0.204, 0.232, 0.237, 0.267, 0.509, 0.631$ and 0.664 samples (the corresponding M_S values at 1.8 K are $\sim 0.011 \mu_B$, $\sim 0.065 \mu_B$, $\sim 0.041 \mu_B$, $\sim 0.064 \mu_B$, $\sim 0.53 \mu_B$, $\sim 0.43 \mu_B$, $\sim 0.19 \mu_B$, and $\sim 0.23 \mu_B$ per formula unit (f.u.) $^{-1}$, respectively). The black arrows indicate the ferrimagnetic transition temperatures (T_{ferri}), defined as the temperatures at $M_S(T) = 0.01 \mu_B (\text{f.u.})^{-1}$ (dashed line). The $\delta = 0.509$ sample contains a magnetic impurity phase of 0.19 at.% Fe_3O_4 . (see figure S3) The Fe_3O_4 contribution is excluded from the $M_S\text{--}T$ curve of this sample. The M_S values of the $\delta = 0.124$ and 0.664 samples are extrapolated to $T = 1.8$ K using the following empirical equation [46]:

$$M_S(T) = M_S(0) \left(1 - \frac{T}{T_{\text{ferri}}}\right)^\alpha \text{ for } 0 \leq \frac{T}{T_{\text{ferri}}} \leq 1,$$

where we assume $\alpha = 0.05\text{--}2.00$. (b) M_S at 1.8 K (closed circles) and T_{ferri} (open circles) versus δ . (c) magnetic SVF versus δ . Inset plots the molar magnetization (M_{mol}) versus $\mu_0 H$ in the $\delta = 0.088$ (red closed circles), 0.124 (blue closed squares), 0.145 (blue open triangles), 0.204 (green open diamonds), 0.237 (green closed triangles) and 0.267 (red open circles) samples at 1.8 K. The solid line indicates the magnetization of perfect diamagnetism, applying the magnetic susceptibility of $\text{Sr}_2\text{VFeAsO}_{3-\delta}$ ($\chi_{\text{mol}} = -5.81$ emu).

representative values obtained by round-up. Widely distributed B_{int} s of Fe were verified in these samples [51, 52] (figure 8(b), insets).

The normally conducting samples ($\delta = 0.267, 0.509$, and 0.631) exhibit AFM phases of the Fe sublattice at $T < \sim 20$ K and M_S at $T < T_{\text{ferri}}$ (308, 297 and 158 K for $\delta = 0.267, 0.509$ and 0.631 , respectively). Such a discrepancy between the T_N of Fe and T_{ferri} indicates that the magnetic phase of the Fe sublattice was uninfluenced by T_{ferri} . Therefore, the T_{ferri} was ascribed to a magnetic phase of the V sublattice. T_{anom} was also irrelevant to the magnetic Fe phase and likely corresponded to the magnetic transition temperature of the V sublattice in $\text{Sr}_2\text{VFeAsO}_{3-\delta}$, T_N and/or the T_{ferri} of V.

3.6. Correlations among thermal, electronic and magnetic properties

Figures 9(a) and (b) show the temperature dependences of the molar heat capacity (C_{mol}) and the excess contribution of the heat capacity (C_{ex}), obtained by subtracting the Debye phonon and Sommerfeld's normally conducting contributions from C_{mol} . Figure 9(c) shows the differential length (ΔL) of the lattice constants (a, c) in the normal conducting $\delta = 0.509$ sample. The C_{ex} is attributable to a transition of the electronic and magnetic phases that predominantly contribute to the thermal properties of solids at low temperatures. The C_{ex} was maximized at $T \approx 10$ K and decreased with increasing T , converging to zero at $T \approx 20$ K. In the $\delta = 0.509$ sample, the $C_{\text{ex}}\text{--}T$ correlated with the magnetic phase transition at the T_N of Fe. The temperature dependences of the lattice constants a and c , which are obtained from the LTXRD patterns, also show an anomalous kink at ~ 10 K (figure 9(c)). The anomalous kink is likely reflecting a local crystallographic structure transition in $\text{Sr}_2\text{VFeAsO}_{3-\delta}$. These results indicate a clear association between the anomalous kink in the (a, c) $\text{--}T$ curves and T_{max} in the $\rho\text{--}T$ curve and a the lattice-formation-enthalpy in $\text{Sr}_2\text{VFeAsO}_{3-\delta}$.

3.7. Element specific electronic and magnetic phase diagrams

Figure 10 plots various temperatures (T_N ($\approx T_{\text{anom}}$), T_{ferri} of V, T_N of Fe, T_{max} , and T_c) as a functions of δ . Finite δ was inevitable in our samples. In the magnetic phase diagram of V in $\text{Sr}_2\text{VFeAsO}_{3-\delta}$, an AFM phase of V sublattice appeared in the $\delta = 0.031\text{--}0.267$ region (figure 10(a)). An AFM phase of V was earlier verified by Tatematsu *et al* [23]. The present samples exhibited a PM phase of the Fe sublattice from 20 to 300 K (figures 7 and S6). The $\delta = 0.124, 0.204, 0.232, 0.237, 0.267, 0.509, 0.631$ and 0.664 samples showed finite M_S at $T < T_{\text{ferri}}$. The T_{ferri} shows maximum at $T = 304$ K in the $\delta = 0.267$ sample and decreased as δ increased above 0.267. Both the AFM and Ferri. phases of V were observed in the $\delta = 0.124\text{--}0.267$ samples, indicating a phase-segregated magnetic state of the V sublattice. Such an inhomogeneous state is an intrinsic property of off-stoichiometric compounds. Indeed, the apparent mixed valence of V is an essential electronic state for a ferrimagnetic V phase in $\text{Sr}_2\text{VFeAsO}_{3-\delta}$.

The $\delta = 0.073$ and $\delta = 0.145$ samples possessed the optimum oxygen deficiencies that maximized the T_{cS} . $\text{Sr}_2\text{VFeAsO}_{3-\delta}$ exhibited a bulk SC phase below the $T_{\text{c}}^{\text{mid}}\text{--}\delta$ curve in the $0.031 \leq \delta \leq 0.145$ range and a normal conducting phase in the $0.204 \leq \delta \leq 0.664$ range, with SC-traces in the $0.204 \leq \delta \leq 0.237$ samples range. The electronic phase segregation, which is mainly induced by inhomogeneous chemical state, is consistent with the inhomogeneous magnetic V states in $\text{Sr}_2\text{VFeAsO}_{3-\delta}$ with $\delta = 0.124\text{--}0.267$. In the $0.031 \leq \delta \leq 0.237$ range, $\text{Sr}_2\text{VFeAsO}_{3-\delta}$ presented a PM

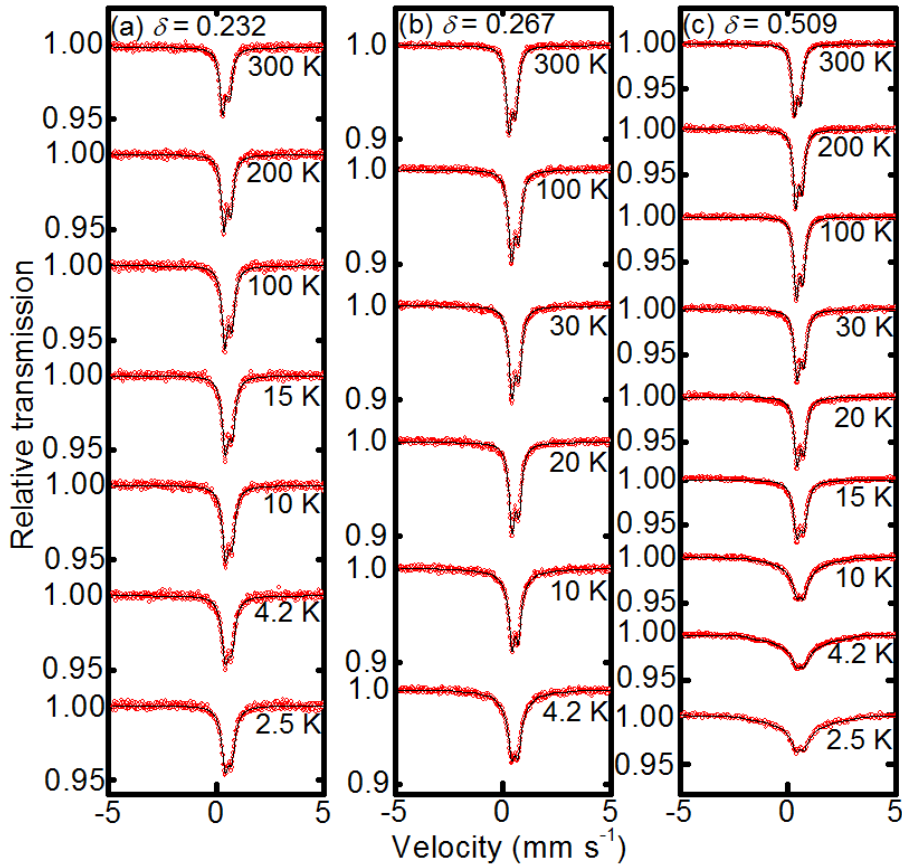


Figure 7. ^{57}Fe MS of representative $\text{Sr}_2\text{VFeAsO}_{3-\delta}$ samples at different temperatures (indicated near the plots). (a) $\delta = 0.232$, (b) $\delta = 0.267$ and (c) $\delta = 0.509$. The solid lines are the fitted patterns to a wide distribution of internal magnetic fields. ^{57}Fe MS are summarized with those of the other samples ($\delta = 0.124$ and $\delta = 0.631$) in figure S7 of the supplementary information.

phase of the Fe sublattice at 2 K. Meanwhile, the normally conducting samples ($\delta = 0.267$, 0.509 , and 0.631) exhibited AFM phases of Fe at $T < \sim 20$ K, indicating no coexisting SC and AFM phases of Fe in the prepared samples.

4. Discussions

4.1. Oxygen deficiencies and molecular (local) structures in the lattice

As shown in figure 3, the lattice volume of $\text{Sr}_2\text{VFeAsO}_{3-\delta}$ expanded with increasing δ , as also observed in perovskite-type and perovskite-related compounds such as $\text{SrTiO}_{3-\delta}$ [53], $\text{YBa}_2\text{Cu}_3\text{O}_{7-\delta}$ [33], and $\text{Bi}_{2.1}\text{Sr}_{1.9}\text{Ca}_2\text{Cu}_3\text{O}_{10+\delta}$ [54]. Such lattice expansion probably characterizes the crystallographic properties of perovskite-related compounds. The average bond valence sum (BVS) [55] of V^{III} , V^{IV} and V^{V} in the $\delta = 0.509$ sample was 2.81, smaller than the average BVS reported by Cao *et al* [24]. The As–Fe–As bond angle (α) in the FeAs layer of this sample was $106.43(9)^\circ$ (see figure 1(b) and table S2 in the supplementary information), indicating that the FeAs₄ tetrahedron was distorted from the regular tetrahedron with $\alpha = 109.47^\circ$ [7, 24].

In the $T_{\text{max}}-\delta$ curve (figure 10), T_{max} was assumed to equal the temperature of a local crystallographic transition,

probed by the anomalous kinks in the $(a, c)-T$ curves of the $\delta = 0.509$ sample. The T_{max} and C_{ex} in this sample probably arose from the local crystallographic phase transition at 10 K (figures 5(a), 9(b) and (c)). A possible local crystallographic transition is consistent with ^{57}Fe MS detailed in section 4 of the supplementary information. For a crystallographic site-specific analysis of 21113 with oxygen deficiencies, further neutron diffraction measurements and Rietveld refinement are required.

4.2. Formation enthalpy differences among magnetic phases in $\delta = 0$ sample

At the optimum δ in $\text{Sr}_2\text{VFeAsO}_{3-\delta}$, superconductivity was activated while the magnetic Fe phase was suppressed (figure 10). This result is consistent with Fermi surface nesting, a theoretical concept proposed by Nakamura *et al* [42], which suggests the emergence of an AFM phase of Fe. A similar relation between the AFM and SC phases of Fe has been reported in the 1111 compounds [2, 50]. The AFM phase of Fe may be understood as a spin density wave. The magnetic ground states of V and the Fe sublattices were quantified in DFT calculations of virtually defined $\text{Sr}_2\text{VFeAsO}_{3-\delta}$ supercells ($\delta = 0, 0.25$ and 0.50) (figures 1(d)–(f)). Table 1 summarizes four different magnetic configurations of the $\delta = 0$ sample and

the total energy of each configuration. The internal coordinates were fixed. The formation enthalpy differences (ΔE) amongst the four configurations reflect the differences in their charge density distributions. The checkerboard-AFM phase (denoted c-AF) of V indicates that the neighboring magnetic V ions on the same layer always have opposite moments. We define the AFM ordering between two neighboring V layers with opposite moments as A-AF on V. A striped-AFM phase of Fe is defined as s-AF on Fe. In the s-AF phase, the magnetic ions on the same layer align in parallel rows, as proposed by Nakamura *et al* [42]. Concordant with their results [42], we referenced ΔE to the most stable structures, c-AF on V and s-AF on Fe. The varying ΔE indicates that several stable solutions were calculated for the same magnetic phase; the ΔE of a magnetic phase are not unique. The lowest energies were 175 meV for [A-AF on V, PM on Fe] and 183 meV for [c-AF on V, PM on Fe], confirming that PM on Fe is not a ground state. In fact, s-AF was the most stable state of Fe. The minimum energy was 4 meV lower in [c-AF on V, s-AF on Fe] than in [A-AF on V, s-AF on Fe]. We concluded that the stability of A-AF and c-AF on V can be altered by slightly changing the chemical composition of $\text{Sr}_2\text{VFeAsO}_{3-\delta}$. Our results partially support the work of Nakamura *et al* [42]. The subtle differences between ours and Nakamura *et al*'s results are caused by the different exchange correlation potentials and/or initial conditions, such as the assumed magnetic moments of V and Fe. These discrepancies would be clarified in further computational analysis on a larger magnetic supercell of $\text{Sr}_2\text{VFeAsO}_{3-\delta}$.

4.3. Formation enthalpy differences among magnetic phases in $\delta = 0, 0.25, 0.50$ samples

Consequent to the above analysis, we defined a ferromagnetic (FM) phase and a Ferri. phase of the V in oxygen deficient supercells. Table 2 summarizes several magnetic configurations of V and their ΔE s in the $\delta = 0, 0.25$ and 0.50 samples, assuming a fixed s-AF magnetic configuration of Fe. In this case, we relaxed the internal coordinates. The relaxation was within 0.02 nm along the c -axis and indiscernible along the other axes. Moreover, the relaxation trends were almost identical amongst the configurations. As shown in the first block of table 2, ΔE s of several magnetic configurations on the V layer (the A-AF, FM, c-AFs and Ferri. phases) were very close. Under oxygen-deficient conditions ($\delta = 0.25$ and 0.50), the magnitude of the magnetic moment of V clearly depended on δ despite the ΔE similarity. When oxygen is removed, V is deprived of its V–O bond in the supercell. Both the A-AF phase of V in the $\delta = 0.25$ sample and the c-AF phase of V in the $\delta = 0.50$ sample showed Ferri. phase behavior. Based on these results, we argue that the d electrons are rather localized around V ions with magnetic moments from $1.9 \mu_B$ to $2.3 \mu_B$. When the magnetic moments of V are sufficiently different, the Ferri. phase of V might be stabilized by magnetic imbalance of the V sublattice. According to our calculations, the magnetic ground states of V in the virtual superlattice of $\text{Sr}_2\text{VFeAsO}_{3-\delta}$ were A-AF in the $\delta = 0$ sample, Ferri. in the $\delta = 0.25$ and 0.50 samples. The calculated stabilities of the magnetic V phases were consistent with the experimental

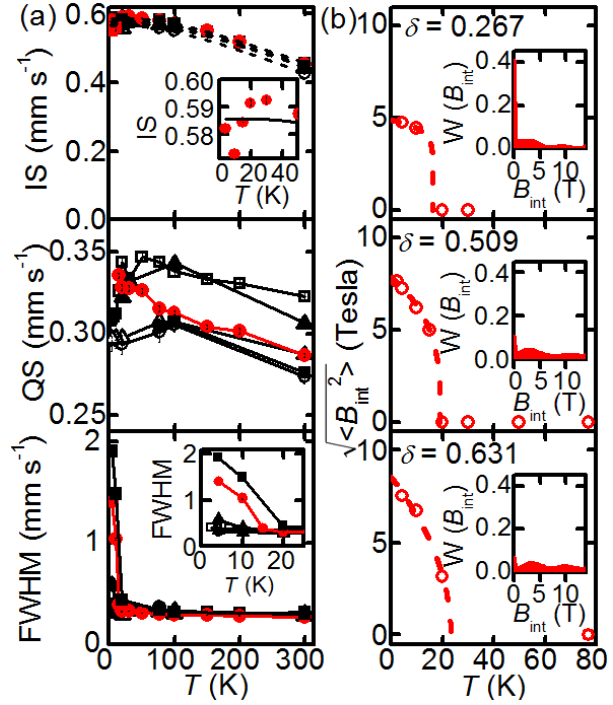


Figure 8. Electronic and magnetic properties of ^{57}Fe in $\text{Sr}_2\text{VFeAsO}_{3-\delta}$. (a) Temperature (T) dependences of the ISs, QS and full width at half maximums (FWHMs) in the $\text{Sr}_2\text{VFeAsO}_{3-\delta}$ samples with $\delta = 0.124$ (open circles), 0.232 (open squares), 0.267 (closed triangles), 0.509 (red closed circles) and 0.631 (closed squares). The QS and FWHM values of the $\delta = 0.267, 0.509$ and 0.631 samples are written only when the spectrum is a doublet. The black lines are the standard deviations. Insets are expanded views of the regular figures. Analytical details are provided in section 4 of the supplementary information. (b) Temperature (T) dependence of the square root of the mean squared amplitude of the internal magnetic field $\sqrt{\langle B_{\text{int}}^2 \rangle}$ obtained from the the internal magnetic field (B_{int}) distributions of the $\delta = 0.267, 0.509$ and 0.631 samples (which exhibited AFM ordering of the Fe sub-lattice at temperatures less than the Néel temperature (T_N)). The red dashed lines are fitted using the following equation [46]:

$$\sqrt{\langle B_{\text{int}}^2 \rangle} = B_0 \left(1 - \frac{T}{T_N}\right)^\alpha \text{ for } 0 \leq \frac{T}{T_N} \leq 1$$

where $\alpha = 0.1-0.5$. Insets show distributed weights as functions of the B_{int} ($W(B_{\text{int}})$) in each sample at 4.2 K.

results of the $\delta \sim 0, \sim 0.25$ and ~ 0.50 samples. As shown in figures 6 and 10 and table 2, the $\delta = 0.267$ sample yielded the largest spontaneous magnetic moment and the highest T_{ferri} .

4.4. Comments on the possible mechanism of the T_c - δ phase diagram and the enhancement of T_c near the ferrimagnetic phase of the vanadium

Magnetic Fe and magnetic V ions exist in a unit cell of $\text{Sr}_2\text{VFeAsO}_{3-\delta}$. The V sublattice of $\text{Sr}_2\text{VFeAsO}_{3-\delta}$ orders antiferromagnetically at $\delta < 0.124$. A weak Ferrimagnetic ordered V sublattice of $\text{Sr}_2\text{VFeAsO}_{3-\delta}$ appears at $\delta \geq 0.124$, and macroscopic spontaneous magnetic moment of the V reaches $\sim 0.5 \mu_B(\text{f.u.})^{-1}$ for $\delta \sim 0.267$ sample (figure 6). Qian

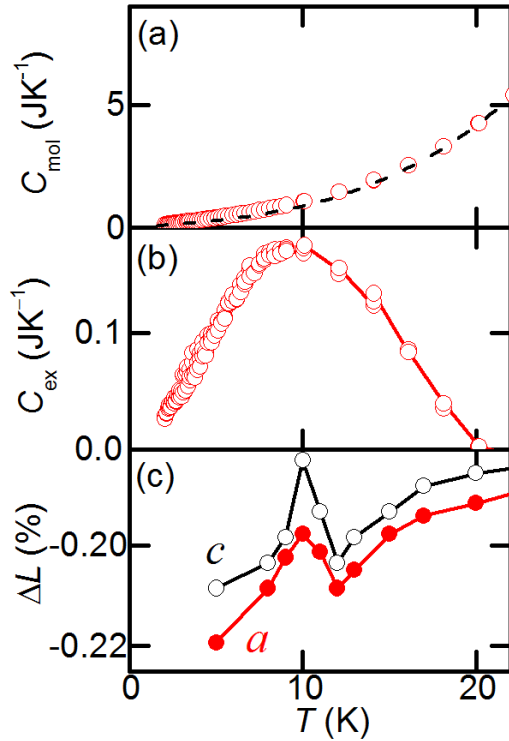


Figure 9. Temperature (T) dependences of molar heat capacity (C_{mol}) (a), excess contribution of heat capacity (C_{ex}) (b) and lattice length change (ΔL) (c) in $\text{Sr}_2\text{VFeAsO}_{3-\delta}$ ($\delta = 0.509$). The dashed line is the best-fits line of $C_{\text{low}} = \gamma T + \beta T^3$, where γ and β are the Sommerfeld coefficient and the lattice heat capacity coefficient, respectively, for the Debye heat capacity at low temperatures ($\gamma = 65.5(3) \text{ mJ K}^{-2} \text{ mol}^{-1}$ and $\beta = 0.52(1) \text{ mJ K}^{-4} \text{ mol}^{-1}$). C_{ex} is calculated as $C_{\text{ex}} = C_{\text{mol}} - C_{\text{low}}$. ΔL is defined as changes of lattice constants (a and c) from the values at 290 K.

et al observed Mott-insulating V $3d$ orbitals with Hubbard gap in SC $\text{Sr}_2\text{VFeAsO}_{3-\delta}$ using angle-resolved x-ray photoemission spectroscopy [56]. According to Qian *et al*'s report, the Mott-insulating V $3d$ orbitals are not hybridized with conducting Fe $3d$ orbitals around Fermi energy, although possible hybridization between the Fe $3d$ and the V $3d$ orbitals should be noted for $\delta \geq 0.124$ samples.

In general, an appearance of the high- T_c SC phase is dominated by appearance of correlated electrons' pairing mediated by both of a phonon [57] and an other driving force [58]. The driving force has been quantitatively explained by so-called t - J model [59, 60] and spin-fluctuation mediated model [61, 62]. Each model have succeeded to demonstrate rational relation between AFM phase and SC phase in high- T_c superconductors. A difference between two models depends on approaches for quantifying stability of SC phases with simple assumption.

For an iron-based superconductor $\text{ReFeAsO}_{1-x}\text{F}_x$, Kuroki *et al* and Mazin *et al* reported that extended s -wave pairing (S_{+-}) with a sign reversal of the order parameter between different Fermi surface sheets [63], assuming multiple spin-fluctuation modes [64]. Kuroki *et al* have succeeded to demonstrate a generic SC phase diagram against a pnictogen height in the $\text{ReFeAsO}_{1-x}\text{F}_x$ [65]. The generic SC phase diagram is in accord to the so-called 'Lee's plot' showing a empirical

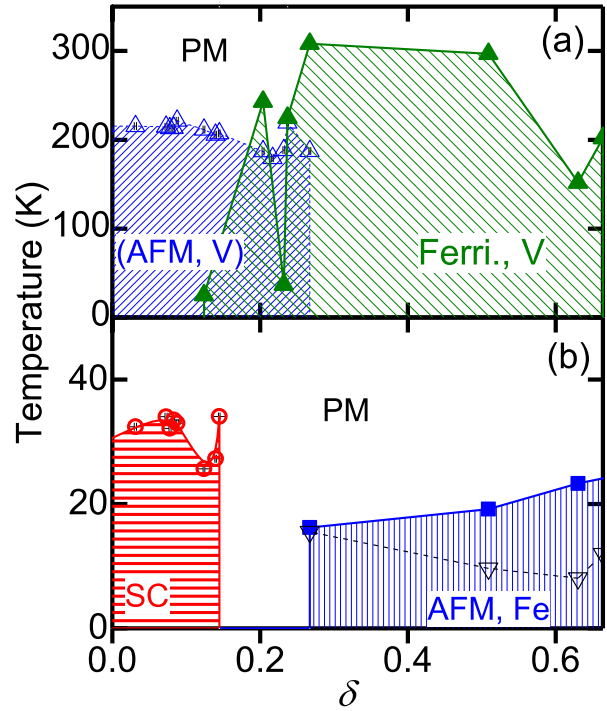


Figure 10. Element-specific electronic and magnetic phase diagrams of $\text{Sr}_2\text{VFeAsO}_{3-\delta}$ in terms of δ and T . (a) Magnetic phase diagram of V. Green closed triangles indicate the ferrimagnetic (Ferri.) phase transition temperatures, at which the spontaneous magnetic moment $M_S(T)$ is equal to $0.01 \mu_B$ (f.u.) $^{-1}$. The green shadowed area indicates a Ferri. phase. The blue open triangles indicate the AFM Néel temperatures (T_N), assuming that T_N appears at $\sim T_{\text{anom}}$ (defined in figure 5), as reported by Tatematsu *et al* [23]. The blue shadowed area indicates an AFM phase. The Ferri. and AFM phases overlap in the region of chemical inhomogeneity, which exhibits SC traces. (b) Electronic and magnetic phase diagrams of Fe in $\text{Sr}_2\text{VFeAsO}_{3-\delta}$. Red open circles indicate T_c^{mid} in bulk SC samples (see table S3 in the supplementary information). The small black lines in the plots are standard deviations. The red and blue shadowed areas indicate the superconducting (SC) phase and AFM phase, respectively, and the blue closed squares indicate T_N determined via ^{57}Fe Mössbauer spectroscopy. Black downward triangles denote the T_{max} values of normally conducting samples, which are probably coupled with transitions in crystallographic local structure.

relation between bonding angles of FeAs_4 molecule and maximum T_c in doped ReFeAsO [66]. Saito *et al* have focused on a discussion for iron-based superconductors' anomalous robustness against various impurities and randomness [67]. Because the anomalous robustness is not explained enough by the spin-fluctuation-mediated model [63, 64], Saito *et al* introduced an orbital fluctuation mediated s -wave state for electrons' pairing in iron-based superconductors. On the other hand, Yamase *et al* reported that an incommensurate magnetic order and d -wave superconductivity coexist in a 2D Hubbard model [68].

Further, Andersen *et al* theoretically reported a mechanism whereby disorder can enhance the T_c of unconventional superconductor with correlated electrons' pairing driven by exchange of spin fluctuation [69, 70]; i.e. iron-based

Table 1. Magnetic moments and formation enthalpy differences (ΔE) relative to the most stable magnetic phase in several magnetic configurations of $\text{Sr}_2\text{VFeAsO}_{3-\delta}$ ($\delta = 0$). The internal coordinates are fixed at their reported values [7].

Order		Moments (μ_B)		ΔE (meV (f.u.) ⁻¹)	
V	Fe	V	Fe	This work	Nakamura <i>et al</i>
A-AF	PM	1.9	0	175–271	766
c-AF	PM	1.9	0	183	58
A-AF	s-AF	1.9	2.2	4–43	—
c-AF	s-AF	1.9	2.2	0–44	0

Table 2. Magnetic moments and formation enthalpy differences (ΔE) relative to the most stable magnetic phases in several magnetic configurations of $\text{Sr}_2\text{VFeAsO}_{3-\delta}$ ($\delta = 0, 0.25$ and 0.50). The internal coordinates are relaxed, and the magnetic phase of Fe is fixed in the s-AF phase.

δ	Order	Moments (μ_B)				ΔE (meV (f.u.) ⁻¹)
		V1	V2	V3	V4	
0	A-AF	-1.9	-1.9	1.9	1.9	0
	FM	1.9	1.9	1.9	1.9	4
	c-AF	-1.9	1.9	-1.9	1.9	4
	c-AF	1.9	-1.9	-1.9	1.9	5
	Ferri.	-1.9	-1.9	1.9	-1.9	16
0.25	Ferri.	1.9	1.9	1.9	-2.2	0
	Ferri.	1.9	1.9	-1.9	-2.3	7
	FM	1.9	1.9	1.9	2.3	10
0.50	Ferri.	1.9	-2.3	1.9	-2.3	0
	FM	1.9	2.3	1.9	2.3	9
	A-AF	-1.9	-2.3	1.9	2.3	29

superconductors. Romer’s report indicated that appropriate amount of lattice defects and randomness possibly enhance the T_c of iron-based superconductors.

In $\text{Sr}_2\text{VFeAsO}_{3-\delta}$, a weak ferrimagnetic V sublattice is observed in a SC sample which exhibits the highest $T_c \sim 37.1$ K at $\delta = 0.145$; i.e. the highest T_c is observed in ‘so-called dirty SC state’. Provided that the Mott-insulating V $3d$ orbitals partially disintegrated in $\delta \geq 0.124$ samples, density of state of magnetic V $3d$ orbitals should modulate the formation of Fermi surfaces and stability of correlated electrons’ pairing for superconductivity in $\text{Sr}_2\text{VFeAsO}_{3-\delta}$. Each theoretical model mentioned above might verify the mechanism for the maximum T_c s at $\delta = 0.078$ and 0.145 in figure 10.

5. Conclusions

We measured the electrical resistivities, magnetic properties and ^{57}Fe MS of well-characterized polycrystalline $\text{Sr}_2\text{VFeAsO}_{3-\delta}$. DFT calculations support several magnetic phases in the V sublattice. Assuming linearity between δ and the lattice volume, we found that changing δ altered a - δ and c - δ curves. Bulk superconductivity was observed in the samples with $0.031 \leq \delta \leq 0.145$ samples. In the range $0.204 \leq \delta \leq 0.664$, the samples were normally conducting

at $T > 2$ K, although SC traces were observed in the range $0.204 \leq \delta \leq 0.237$. These SC-traces were mainly attributable to chemical phase segregation. The highest T_c^{onset} and T_c^{mid} were observed at 37.1 K and 34.1 K respectively, in the $\delta = 0.145$ sample. A spontaneous magnetic moment (M_S) of V appears in the $0.124 \leq \delta \leq 0.631$. M_S exhibits a maximum value $\sim 0.5 \mu_B$ (f.u.)⁻¹ in the $\delta = 0.267$ sample. The $0.124 \leq \delta \leq 0.631$ samples exhibit a wide range of magnetic V transition temperatures (25–308 K). The ^{57}Fe MS of $\text{Sr}_2\text{VFeAsO}_{3-\delta}$ verified PM phase in the Fe sublattice of the SC $\delta = 0.124$ sample and in the normally conducting samples with $\delta = 0.232$ and 0.237 . The AFM phases of Fe appear at $T < 16.2(4)$ K, $19.2(4)$ K and $23.3(4)$ K in the $\delta = 0.267, 0.509,$ and 0.631 samples, respectively. According to our DFT calculations, the stable AFM phase of V can be altered by varying δ (because the formation enthalpies of the various magnetic phases are quite similar); moreover, the Ferri. phase of V is stable when $\delta = 0.25$ and 0.50 samples. Based on these results, we constructed an electronic and magnetic phase diagram of $\text{Sr}_2\text{VFeAsO}_{3-\delta}$ with respect to δ . This phase diagram verified the lack of coexisting AFM and SC phases in the Fe sublattice, although the maximum T_c was raised near the AFM-Ferri. phases boundaries of V. The magnetic and valence states of V indirectly dominate the T_c of $\text{Sr}_2\text{VFeAsO}_{3-\delta}$. Through this phase diagram, we can better understand the chemical compositions that optimise the superconductivity of iron-based MALCs and thus develop mechanisms for enhancing T_c in multinary transition metals-based MALCs, which are promising materials for SC applications under high magnetic fields.

This article contains supplementary information online referring to [71–93].

Acknowledgments

This work was supported by the research grant of Keio University, the Sumitomo foundation, and the Ministry of Education, Culture, Sports, Science, and Technology (MEXT) through the Element Strategy Initiative to Form Core Research Center. This work used the facilities of the Institute for Integrated Radiation and Nuclear Science, Kyoto University, and was supported in part by the Collaborative Research Project of Laboratory for Materials and Structures, Tokyo Institute of Technology. We thank D Ikuta for help with the XRD experiments. This research was partially funded by the US Department of Energy (DOE), Office of Basic Energy Sciences (BES). SH and WLM are supported by DOE, Office of Basic Energy Sciences (BES), Division of Materials Sciences and Engineering, under Contact No. DE-AC02-76SF00515. H Hi was also supported by the Japan Society for the Promotion of Science (JSPS) through a Grant-in-Aid for Scientific Research on Innovative Areas ‘Nano Informatics’ (Grant Number 25106007), a Grant-in-Aid for Scientific Research (A) (grant no. 17H01318) and Support for Tokyotech Advanced Research (STAR). YK was also supported by the JSPS through a Grant-in-Aid for Scientific Research (A) (grant no. 15H01998), (B) (grant no. 17H03239, 18H01163), and Core-to-Core Program ‘Isotope spintronics’.

ORCID iDs

Hidenori Hiramatsu  <https://orcid.org/0000-0002-5664-5831>

Yoichi Kamihara  <https://orcid.org/0000-0002-6871-171X>

References

- [1] Kamihara Y, Watanabe T, Hirano M and Hosono H 2008 Iron-based layered superconductor $\text{La}[\text{O}_{1-x}\text{F}_x]\text{FeAs}$ ($x = 0.05\text{--}0.12$) with $T_c = 26$ K *J. Am. Chem. Soc.* **130** 3296–7
- [2] Kamihara Y and Hosono H 2016 Superconductivity in iron oxypnictide induced by F-doping *Photonic and Electronic Properties of Fluoride Materials* ed A Tressaud and K Poeppelmeier (Amsterdam: Elsevier) pp 423–46
- [3] Shimoyama J 2014 Potentials of iron-based superconductors for practical future materials *Supercond. Sci. Technol.* **27** 044002
- [4] Stewart G-R 2011 Superconductivity in iron compounds *Rev. Mod. Phys.* **83** 1589–652
- [5] Hosono H and Kuroki K 2015 Iron-based superconductors: current status of materials and pairing mechanism *Physica C* **514** 399–422
- [6] Ogino H, Matsumura Y, Katsura Y, Ushiyama K, Horii S, Kishio K and Shimoyama J 2009 Superconductivity at 17 K in $(\text{Fe}_2\text{P}_2)(\text{Sr}_4\text{Sc}_2\text{O}_6)$: a new superconducting layered pnictide oxide with a thick perovskite oxide layer *Supercond. Sci. Technol.* **22** 075008
- [7] Zhu X, Han F, Mu G, Cheng P, Shen B, Zeng B and Wen H 2009 Transition of stoichiometric $\text{Sr}_2\text{VO}_3\text{FeAs}$ to a superconducting state at 37.2 K *Phys. Rev. B* **79** 220512
- [8] Ogino H, Katsura Y, Horii S, Kishio K and Shimoyama J 2009 New iron-based arsenide oxides $(\text{Fe}_2\text{As}_2)(\text{Sr}_4\text{M}_2\text{O}_6)$ ($\text{M} = \text{Sc}, \text{Cr}$) *Supercond. Sci. Technol.* **22** 085001
- [9] Xie Y L *et al* 2009 Structure and physical properties of the new layered oxypnictides $\text{Sr}_4\text{Sc}_2\text{O}_6\text{M}_2\text{As}_2$ ($\text{M} = \text{Fe}$ and Co) *Europhys. Lett.* **86** 57007
- [10] Chen G F, Xia T L, Yang H X, Li J Q, Zheng P, Luo J L and Wang N L 2009 Possible high temperature superconductivity in a Ti-doped A-Sc-Fe-As-O ($\text{A} = \text{Ca}, \text{Sr}$) system *Supercond. Sci. Technol.* **22** 072001
- [11] Zhang S B, Guo Y F, Shi Y G, Yu S, Li J J, Wang X X, Arai M, Yamaura K and Takayama-Muromachi E 2011 Magnetic and electrical properties and carrier doping effects on the iron-based host compound $\text{Sr}_2\text{ScFeAsO}_3$ *Phys. Rev. B* **83** 024505
- [12] Tegel M, Hummel F, Lackner S, Schellenberg I, Pöttgen R and Johrendt D 2009 The layered iron arsenide oxides $\text{Sr}_2\text{CrO}_3\text{FeAs}$ and $\text{Ba}_2\text{ScO}_3\text{FeAs}$ *Z. Anorg. Allg. Chem.* **635** 2242–8
- [13] Zhu X, Han F, Mu G, Cheng P, Shen B, Zeng B and Wen H 2009 Superconductivity in Ti-doped iron-arsenide compound $\text{Sr}_4\text{Cr}_{0.8}\text{Ti}_{1.2}\text{O}_6\text{Fe}_2\text{As}_2$ *Sci. China G* **52** 1876–8
- [14] Sato S, Ogino H, Kawaguchi N, Katsura Y, Kishio K, Shimoyama J, Kotegawa H and Tou H 2010 Superconductivity in a new iron pnictide oxide $(\text{Fe}_2\text{As}_2)(\text{Sr}_4(\text{Mg}, \text{Ti})_2\text{O}_6)$ *Supercond. Sci. Technol.* **23** 045001
- [15] Shirage P M, Kihou K, Lee C, Kito H, Eisaki H and Iyo A 2010 Superconductivity at 28.3 and 17.1 K in $(\text{Ca}_4\text{Al}_2\text{O}_{6-y})(\text{Fe}_2\text{Pn}_2)$ ($\text{Pn} = \text{As}$ and P) *Appl. Phys. Lett.* **97** 172506
- [16] Zhu X, Han F, Mu G, Shen B, Cheng P, Zeng B and Wen H 2009 $\text{Sr}_3\text{Sc}_2\text{Fe}_2\text{As}_2\text{O}_5$ as a possible parent compound for FeAs-based superconductors *Phys. Rev. B* **79** 024516
- [17] Tegel M, Schellenberg I, Hummel F, Pöttgen R and Johrendt D 2009 Low-temperature crystal structure and ^{57}Fe Mössbauer spectroscopy of $\text{Sr}_3\text{Sc}_2\text{O}_5\text{Fe}_2\text{As}_2$ *Z. Naturforsch. B* **64** 815–20
- [18] Ogino H, Sato S, Kishio K, Shimoyama J, Tohei T and Ikuhara Y 2010 Homologous series of iron pnictide oxide superconductors $(\text{Fe}_2\text{As}_2)[\text{Ca}_{n+1}(\text{Sc}, \text{Ti})_n\text{O}_y]$ ($n = 3, 4, 5$) with extremely thick blocking layers *Appl. Phys. Lett.* **97** 072506
- [19] Ogino H, Machida K, Yamamoto A, Kishio K, Shimoyama J, Tohei T and Ikuhara Y 2010 A new homologous series of iron pnictide oxide superconductors $(\text{Fe}_2\text{As}_2)(\text{Ca}_{n+2}(\text{Al}, \text{Ti})_n\text{O}_y)$ ($n = 2, 3, 4$) *Supercond. Sci. Technol.* **23** 115005
- [20] Han F, Zhu X, Mu G, Cheng P, Shen B, Zeng B and Wen H 2010 Structural and transport properties of $\text{Sr}_2\text{VO}_{3-\delta}\text{FeAs}$ superconductors with different oxygen deficiencies *Sci. China G* **53** 1202–6
- [21] Kotegawa H, Kawazoe T, Tou H, Murata K, Ogino H, Kishio K and Shimoyama J 2009 Contrasting pressure effects in $\text{Sr}_2\text{VFeAsO}_3$ and $\text{Sr}_2\text{ScFePO}_3$ *J. Phys. Soc. Japan* **78** 123707
- [22] Tegel M, Schmid T, Stürzer T, Egawa M, Su Y, Senyshyn A and Johrendt D 2010 Possible magnetic order and suppression of superconductivity by V doping in $\text{Sr}_2\text{VO}_3\text{FeAs}$ *Phys. Rev. B* **82** 140507
- [23] Tatematsu S, Satomi E, Kobayashi Y and Sato M 2010 Magnetic ordering in V-layers of the superconducting system of $\text{Sr}_2\text{VFeAsO}_3$ *J. Phys. Soc. Japan* **79** 123712
- [24] Cao G-H *et al* 2010 Self-doping effect and successive magnetic transitions in superconducting $\text{Sr}_2\text{VFeAsO}_3$ *Phys. Rev. B* **82** 104518
- [25] Corkett A J, Free D-G, Cassidy S-J, Ramos S and Clarke S-J 2014 Control of the superconducting properties of $\text{Sr}_{2-x}\text{Ca}_x\text{VO}_3\text{FeAs}$ through isovalent substitution *J. Solid State Chem.* **216** 91–8
- [26] Munevar J *et al* 2011 Static magnetic order of $\text{Sr}_4\text{A}_2\text{O}_6\text{Fe}_2\text{As}_2$ ($\text{A} = \text{Sc}$ and V) revealed by Mössbauer and muon spin relaxation spectroscopies *Phys. Rev. B* **84** 024527
- [27] Hummel F, Su Y, Senyshyn A and Johrendt D 2013 Weak magnetism and the Mott state of vanadium in superconducting $\text{Sr}_2\text{VO}_3\text{FeAs}$ *Phys. Rev. B* **88** 144517
- [28] Tegel M, Hummel F, Su Y, Chatterji T, Brunelli M and Johrendt D 2010 Non-stoichiometry and the magnetic structure of $\text{Sr}_2\text{CrO}_3\text{FeAs}$ *Europhys. Lett.* **89** 37006
- [29] Pal A, Vajpayee A, Meena R S, Kishan H and Awana V-P-S 2009 Single-step synthesis of $\text{Sr}_4\text{V}_2\text{O}_6\text{Fe}_2\text{As}_2$: the blocking layer based potential future superconductor *J. Supercond. Novel Magn.* **22** 619–21
- [30] Kitao S, Kobayashi Y, Higashitaniguchi S, Saito M, Kamihara Y, Hirano M, Mitsui T, Hosono H and Seto M 2008 Spin ordering in LaFeAsO and its suppression in superconductor $\text{LaFeAsO}_{0.89}\text{F}_{0.11}$ probed by Mössbauer spectroscopy *J. Phys. Soc. Japan* **77** 103706
- [31] Hess C, Kondrat A, Narduzzo A, Hamann-Borrero J E, Klingeler R, Werner J, Behr G and Büchner B 2009 The intrinsic electronic phase diagram of iron-oxypnictide superconductors *Europhys. Lett.* **87** 17005
- [32] Iimura S, Matsuishi S, Sato H, Hanna T, Muraba Y, Kim S W, Kim J E, Takata M and Hosono H 2012 Two-dome structure in electron-doped iron arsenide superconductors *Nat. Commun.* **3** 943
- [33] Kishio K, Shimoyama J, Hasegawa T, Kitagawa K and Fueki K 1987 Determination of oxygen nonstoichiometry in a high- T_c superconductor $\text{Ba}_2\text{YCu}_3\text{O}_{7-\delta}$ *Japan. J. Appl. Phys.* **26** L1228–30
- [34] Burllet P, Vettier C, Jurgens M J G M, Henry J-Y, Rossat-Mignod J, Noel N, Potel M, Gougeon P and Levet J-C 1988 Neutron scattering study of the antiferromagnetic ordering in $\text{YBa}_2\text{Cu}_3\text{O}_{6+x}$ powder and single crystal samples *Physica C* **153–5** 1115–20

- [35] Cava R-J, Hewat A W, Hewat E A, Batlogg B, Marezio M, Rabe K M, Krajewski J J, Peck W-F Jr and Rupp L W Jr 1990 Structural anomalies, oxygen ordering and superconductivity in oxygen deficient $\text{Ba}_2\text{YCu}_3\text{O}_x$ *Physica C* **165** 419–33
- [36] Cox A and Sangster M J L 1985 Vegard's rule and volumes of formation for impurity ions *J. Phys. C: Solid State Phys.* **18** L1123–6
- [37] Goodenough J B 1969 Descriptions of outer d electrons *J. Phys. Chem. Solids* **30** 261–80
- [38] Izumi F and Momma K 2007 Three-dimensional visualization in powder diffraction *Solid State Phenom.* **130** 15–20
- [39] Perdew J, Burke K and Ernzerhof M 1996 Generalized gradient approximation made simple *Phys. Rev. Lett.* **77** 3865–8
- [40] Kresse G and Furthmüller J 1996 Efficient iterative schemes for *ab initio* total-energy calculations using a plane-wave basis set *Phys. Rev. B* **54** 11169–86
- [41] Kresse G and Furthmüller J 1996 Efficiency of *ab-initio* total energy calculations for metals and semiconductors using a plane-wave basis set *Comput. Mater. Sci.* **6** 15–50
- [42] Nakamura H and Machida M 2010 Magnetic ordering in blocking layer and highly anisotropic electronic structure of high- T_c iron-based superconductor $\text{Sr}_2\text{VFeAsO}_3$: LDA+ U study *Phys. Rev. B* **82** 094503
- [43] Blöchl P E 1994 Projector augmented-wave method *Phys. Rev. B* **50** 17953–79
- [44] Liechtenstein A, Anisimov V and Zaanen J 1995 Density-functional theory and strong interactions: orbital ordering in Mott–Hubbard insulators *Phys. Rev. B* **52** 5467–70
- [45] Suetin D, Shein I and Ivanovskii A 2012 The influence of oxygen deficiency on structural and electronic properties of layered superconductor $(\text{Fe}_2\text{As}_2)(\text{Sr}_4\text{V}_2\text{O}_{6-x})$ *J. Mater. Sci.* **47** 3663–8
- [46] Błachowski A, Ruebenbauer K, Żukrowski J, Rogacki K, Bukowski Z and Karpinski J 2011 Shape of spin density wave versus temperature in AFe_2As_2 ($\text{A} = \text{Ca}, \text{Ba}, \text{Eu}$): a Mössbauer study *Phys. Rev. B* **83** 134410
- [47] Gol'danskii V I, Makarov E-F and Khrapov V-V 1963 On the difference in two peaks of quadrupole splitting in Mössbauer spectra *Phys. Lett.* **3** 344–6
- [48] Rotter M, Tegel M and Johrendt D 2008 Spin-density-wave anomaly at 140 K in the ternary iron arsenide BaFe_2As_2 *Phys. Rev. B* **78** 020503
- [49] Hesse J and Rübartsch A 1974 Model independent evaluation of overlapped Mössbauer spectra *J. Phys. E: Sci. Instrum.* **7** 526–32
- [50] Kamihara Y *et al* 2010 Electronic and magnetic phase diagram of superconductors, $\text{SmFeAsO}_{1-x}\text{F}_x$ *New J. Phys.* **12** 033005
- [51] Fawcett E, Alberts H L, Galkin V Y, Noakes D R and Yakhmi J V 1994 Spin-density-wave antiferromagnetism in chromium alloys *Rev. Mod. Phys.* **66** 25–127
- [52] Rivas A, Gonzalez-Jimenez F, D'Onofrio L, Jaimes E, Quintero M and Gonzalez J 2001 SDW in the 2D compound CuFeTe_2 *Hyperfine Interact.* **134** 115–22
- [53] Gong W, Yun H, Ning Y B, Greedan J E, Datars W R and Stagers C V 1991 Oxygen-deficient SrTiO_{3-x} , $x = 0.28, 0.17, \text{ and } 0.08$. Crystal growth, crystal structure, magnetic, and transport properties *J. Solid State Chem.* **90** 320–30
- [54] Watanabe T, Fujii T and Matsuda A 2003 Structural study of inhomogeneous charge distribution of inequivalent CuO_2 planes in $\text{Bi}_{2.1}\text{Sr}_{1.9}\text{Ca}_2\text{Cu}_3\text{O}_{10+\delta}$ single crystals *J. Phys. Soc. Japan* **72** 2924–9
- [55] Brown I D and Altermatt D 1985 Bond-valence parameters obtained from a systematic analysis of the inorganic crystal structure database *Acta Crystallogr. B* **41** 244–7
- [56] Qian T *et al* 2011 Quasinested Fe orbitals versus Mott-insulating V orbitals in superconducting $\text{Sr}_2\text{VFeAsO}_3$ as seen from angle-resolved photoemission *Phys. Rev. B* **83** 140513
- [57] Bardeen J, Cooper L N and Schrieffer J-R 1957 Theory of superconductivity *Phys. Rev.* **108** 1175–204
- [58] Aoki H 2009 *Introduction to Superconductivity* (Tokyo: Shokabo Co., Ltd) pp 110–26 (in Japanese)
- [59] Anderson P W 1987 The resonating valence bond state in La_2CuO_4 and superconductivity *Science* **235** 1196–8
- [60] Scalapino D J 2012 A common thread: The pairing interaction for unconventional superconductors *Rev. Mod. Phys.* **84** 1383–417
- [61] Moriya T, Takahashi Y and Ueda K 1990 Antiferromagnetic spin fluctuations and superconductivity in two-dimensional metals—a possible model for high T_c oxides *J. Phys. Soc. Japan* **59** 2905–15
- [62] Moriya T 2006 Developments of the theory of spin fluctuations and spin fluctuation-induced superconductivity *Proc. Japan. Acad. B* **82** 1–15
- [63] Mazin I I, Singh D J, Johannes M D and Du M H 2008 Unconventional superconductivity with a sign reversal in the order parameter of $\text{LaFeAsO}_{1-x}\text{F}_x$ *Phys. Rev. Lett.* **101** 057003
- [64] Kuroki K, Onari S, Arita R, Usui H, Tanaka Y, Kontani H and Aoki H 2008 Unconventional pairing originating from the disconnected fermi surfaces of superconducting $\text{LaFeAsO}_{1-x}\text{F}_x$ *Phys. Rev. Lett.* **101** 087004
- [65] Kuroki K, Usui H, Onari S, Arita R and Aoki H 2009 Pnictogen height as a possible switch between high- T_c nodeless and low- T_c nodal pairings in the iron-based superconductors *Phys. Rev. B* **79** 224511
- [66] Lee C H, Iyo A, Eisaki H, Kito H, Fernandez-Diaz M T, Ito T, Kihou K, Matsuhata H, Braden M and Yamada K 2008 Effect of structural parameters on superconductivity in fluorine-free LnFeAsO_{1-y} ($\text{Ln} = \text{La}, \text{Nd}$) *J. Phys. Soc. Japan* **77** 083704
- [67] Saito T, Onari S and Kontani H 2010 Orbital fluctuation theory in iron pnictides: effects of As–Fe–As bond angle, isotope substitution, and Z^2 -orbital pocket on superconductivity *Phys. Rev. B* **82** 144510
- [68] Yamase H, Eberlein A and Metzner W 2016 Coexistence of incommensurate magnetism and superconductivity in two-dimensional Hubbard model *Phys. Rev. Lett.* **116** 096402
- [69] Rømer A-T, Hirschfeld P J and Andersen B M 2018 Raising the critical temperature by disorder in unconventional superconductors mediated by spin fluctuations *Phys. Rev. Lett.* **121** 027002
- [70] Gastiasoro M N and Andersen B M 2018 Enhancing superconductivity by disorder *Phys. Rev. B* **98** 184510
- [71] Tojo Y, Matoba M and Kamihara Y 2013 Annealing induced superconductivity in perovskite-related iron-based mixed anion compounds $\text{Sr}_2\text{VFeAsO}_{3-\delta}$ *J. App. Phys.* **113** 17E157
- [72] Katagiri T and Sasagawa T 2013 Crystal growth and anisotropic superconducting properties of $\text{Sr}_2\text{VFeAsO}_3$ *Physica C* **484** 16–8
- [73] Iwasaki S, Matoba M and Kamihara Y 2018 Superconducting critical current densities for $\text{Sr}_2\text{VFeAsO}_{3-\delta}$ wires fabricated by *ex situ* powder-in-tube process *Mater. Sci. Tech. Japan.* **55** 77–81
- [74] Ok J M *et al* 2017 Frustration-driven C_4 symmetric order in a naturally-heterostructured superconductor $\text{Sr}_2\text{VO}_3\text{FeAs}$ *Nat. Commun.* **8** 2167
- [75] Hirai S *et al* 2018 Oxygen vacancy-originated highly active electrocatalysts for the oxygen evolution reaction *J. Mater. Chem. A* **6** 15102–9

- [76] Horio M *et al* 2018 Local magnetic states of the weakly ferromagnetic iron-based superconductor $\text{Sr}_2\text{VFeAsO}_{3-\delta}$ studied by x-ray magnetic circular dichroism *J. Phys. Soc. Japan* **87** 105001
- [77] Sefat A S, Singh D J, Garlea V O, Zuev Y L, McGuire M-A and Sales B-C 2011 Variation of physical properties in the nominal $\text{Sr}_4\text{V}_2\text{O}_6\text{Fe}_2\text{As}_2$ *Physica C* **471** 143–9
- [78] Mazin I I 2010 $\text{Sr}_2\text{VO}_3\text{FeAs}$ as compared to other iron-based superconductors *Phys. Rev. B* **81** 020507
- [79] Lee K W and Pickett W E 2010 $\text{Sr}_2\text{VO}_3\text{FeAs}$: a nanolayered bimetallic iron pnictide superconductor *Europhys. Lett.* **89** 57008
- [80] Ueshima K, Han F, Zhu X, Wen H H, Kawasaki S and Zheng G 2014 Magnetism and superconductivity in $\text{Sr}_2\text{VFeAsO}_3$ revealed by ^{75}As - and ^{51}V -NMR under elevated pressures *Phys. Rev. B* **89** 184506
- [81] Che R C, Han F, Liang C Y, Zhao X B and Wen H H 2014 Microstructural evolution and its influence on the superconductivity induced by oxygen vacancies in $\text{Sr}_2\text{VO}_{3-\delta}\text{FeAs}$ ($\delta = 0.1, 0.5$) *Phys. Rev. B* **90** 104503
- [82] Choi S *et al* 2017 Switching magnetism and superconductivity with spin-polarized current in iron-based superconductor *Phys. Rev. Lett.* **119** 227001
- [83] Fifield F W and Haines P J (ed) 2000 Analytical chemistry *Environmental Analytical Chemistry* (Malden: Blackwell) pp 3–5
- [84] Izumi I, Kiyotaki F, Yagi N, Vlaicu A-M, Nisawa A, Fukushima I, Yoshitake H and Iwasawa Y 2005 X-ray absorption fine structure combined with x-ray fluorescence spectrometry. Part 15. Monitoring of vanadium site transformations of titania and in mesoporous titania by selective detection of the vanadium $K\alpha_1$ fluorescence *J. Phys. Chem. B* **109** 14884–91
- [85] Yasuda S and Kakiyama H 1978 X-ray K emission spectra of vanadium in various oxidation states *X-Ray Spectrom.* **7** 23–5
- [86] Salem S I, Chang C N and Nash T J 1978 Energy shift and structure of the K-absorption edge of vanadium in some vanadium compounds *Phys. Rev. B* **18** 5168–73
- [87] Goldstein J I, Lyman C E, Newbury D E, Lifshin E, Echlin P, Sawyer L, Joy D C and Michael J R 2003 The approach to x-ray quantitation: the need for matrix corrections *Scanning Electron Microscopy and X-ray Microanalysis* 3rd edn (New York: Springer) pp 402–3
- [88] Gorter C J and Casimir H B G 1934 Zur thermodynamik des supraleitenden zustandes *Phys. Z* **35** 963–9
- [89] Gyorgy E M, van Dover R B, Jackson K A, Schneemeyer L F and Waszczak J V 1989 Anisotropic critical currents in $\text{Ba}_2\text{YCu}_3\text{O}_7$ analyzed using an extended Bean model *Appl. Phys. Lett.* **55** 283–5
- [90] Wertheim G K, Buchanan D N E and Guggenheim H J 1970 Thermal shift of a Mössbauer gamma ray at a magnetic phase transition *Phys. Rev. B* **2** 1392–5
- [91] Fujita E, Nasu S, Nishida T and Yoshida Y 2002 Quadrupole splitting *Introduction of Mössbauer Spectroscopy* (Tokyo: Gijyutsu Kyokai Ltd) pp 21–4 (in Japanese)
- [92] Ingalls R I 1964 Electric-field gradient tensor in ferrous compounds *Phys. Rev.* **133** A787–95
- [93] Barrow G M 1996 Crystal and liquid heat capacities *Physical Chemistry* 6th edn (New York: MacGraw-Hill) pp 138–45